Biophysical Journal Volume 82 May 2002 2548–2564

Measurement of Thin Filament Lengths by Distributed Deconvolution Analysis of Fluorescence Images

Ryan Littlefield and Velia M. Fowler
Department of Cell Biology, The Scripps Research Institute, La Jolla, California 92037 USA

ABSTRACT The lengths of the actin (thin) filaments in sarcomeres directly influence the physiological properties of striated muscle. Although electron microscopy techniques provide the highest precision and accuracy for measuring thin filament lengths, significant obstacles limit their widespread use. Here, we describe distributed deconvolution, a fluorescence-based method that determines the location of specific thin filament components such as tropomodulin (Tmod) or probes such as phallacidin (a phalloidin derivative). Using Tmod and phallacidin fluorescence, we were able to determine the thin filament lengths of isolated chicken pectoralis major myofibrils with an accuracy and precision comparable to electron microscopy. Additionally, phallacidin fluorescence intensity at the Z line provided information about the width of Z lines. Furthermore, we detected significant variations in thin filaments lengths among individual myofibrils from chicken posterior latissimus dorsai and embryonic chick cardiac myocytes, suggesting that a ruler molecule (e.g., nebulin) does not strictly determine thin filament lengths in these muscles. This versatile method is applicable to myofibrils in living cells that exhibit significant variation in sarcomere lengths, and only requires a fluorescence microscope and a CCD camera.

INTRODUCTION

The myosin (thick) and actin (thin) filaments of striated muscle produce efficient contractile force because they have well-defined lengths and are organized into regular, symmetric arrays that interdigitate and slide past each other during contraction (Squire, 1997; Huxley, 1963) (see Fig. 1). The thick and thin filaments do not change appreciably in length during contraction (Sosa et al., 1994; Huxley, 1963). However, their lengths are important aspects of muscle physiology because a sarcomere generates force in proportion to thick and thin filament overlap (see Squire, 1997). Consistent with this role, the relative lengths of thick and thin filaments vary according to the physiological requirements of the muscle (van Leeuwen, 1991; Burkholder and Lieber, 2001). In particular, for vertebrates, thick filament lengths are a constant 1.65 μm (Page and Huxley, 1963; Trombitas et al., 1993; Granzier et al., 1991), whereas thin filament lengths vary for different muscle types (Granzier et al., 1991; Kruger et al., 1991; Burkholder and Lieber, 2001). Furthermore, it has been suggested that cardiac thin filament lengths vary within an individual sarcomere due to the physiological requirements of the heart (Robinson and Winegrad, 1979). Together, this suggests that muscle physiology may influence the specification of thin filament lengths. However, to explore a potential relationship between thin filament lengths and muscle physiology, it is imperative to have a rapid method to accurately measure thin filament lengths under a variety of conditions.

Electron microscopy (EM) typically measures thin filament lengths with a high degree of precision and accuracy. However, EM is not applicable to the study of living cells or myofibril dynamics because of the fixation procedures required to preserve the sample for visualization in the electron microscope. Furthermore, procedures such as dehydration, embedding, myosin extraction, and negative staining, may introduce artifacts that are difficult to correct for, including sample shrinkage (Page and Huxley, 1963). Recent advances in image-analysis techniques have raised the possibility that thin filament lengths may be accurately measured by fluorescence microscopy (Agard et al., 1989). Fluorescence microscopy is less invasive than electron microscopy and can be applied to living cells through the use of green fluorescent protein–fusion proteins or fluorescence analog cytochemistry.

We developed a new fluorescence microscopy procedure, distributed deconvolution, which computationally models fluorescent-stained myofibrils and measures their thin filament lengths. This method is distinct from other deconvolution procedures because it uses multivariate line-fitting algorithms rather than Fourier-based algorithms to determine the individual component functions. The method takes advantage of the regular organization of thin filaments into symmetric thin filament arrays (Fig. 1). Thin filament arrays (previously referred to as "I-Z-I bodies" or "I-Z-I complexes," see Holtzer et al., 1997) are arranged in tandem along the myofibril and only move relative to each other when sarcomere lengths change. The thin filament arrays include the major thin filament components (actin, tropomyosin, troponins), proteins at the Z line (e.g., α-actinin and cap Z), and tropomodulin (Tmod) at the slow-growing (pointed) ends of the thin filaments (Littlefield and Fowler, 1998). Distributed deconvolution is capable of modeling the fluorescence from nearly any myofibril component, including, but not limited to, proteins located at thin filament ends or along the length of thin filaments. Here, we use chicken myofibrils costained for Tmod and for actin with phallaci-

Submitted July 2, 2001 and accepted for publication January 2, 2002.
Address reprint requests to Ryan Littlefield, The Salk Institute, 10010 N. Torrey Pines Rd., La Jolla, CA 92037. Tel.: 858-453-4100 x2029; Fax: 858-452-3683; E-mail: littlefield@salk.edu.

0006-3495/02/05/2548/17 $2.00

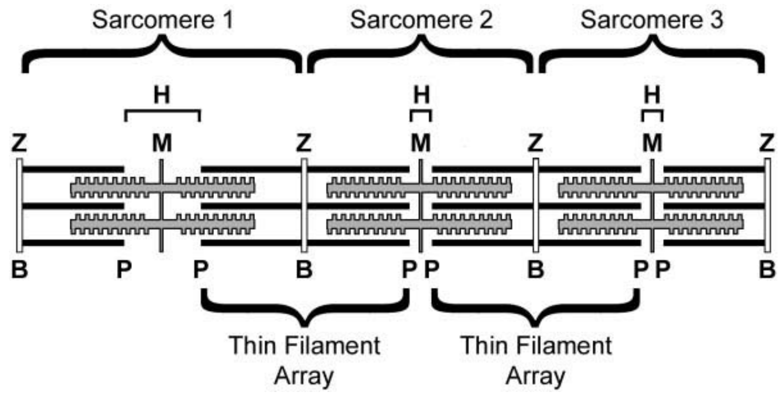

FIGURE 1 Thin filament organization in striated myofibrils. Schematic diagram of three sarcomeres and the symmetric thin filament arrays shared between them. *Z*, Z lines; *M*, M lines; *H*, H zones; *P*, thin filament pointed ends; *B*, thin filament barbed ends. The structure of thin filament arrays remains the same in long (*left*) and short (*middle*, *right*) sarcomeres.

din to measure thin filament length by distributed deconvolution analysis. We found that Tmod is a better probe than phallacidin for measuring thin filament lengths and that the thin filament lengths vary approximately 10–15% for individual myofibrils from posterior latissimus dorsai (PLD) muscle and for embryonic cardiac myocytes.

METHODS

Preparation and staining of isolated myofibrils and cardiac myocytes

Isolated chicken pectoralis major (PM) and PLD myofibrils were prepared according to Knight and Trinick (1982) (see Fowler et al., 1993). Briefly, strips of muscle were stretched with string, tied to plastic syringe plungers, and immersed in an EGTA-Ringer's relaxing buffer (100 mM NaCl, 2mM KCl, 2mM $MgCl_2$, 6 mM potassium phosphate, 1 mM EGTA, 0.1% glucose, pH 7.0 at 0°) overnight at 4°C. Myofibrils were then stored in rigor buffer (100 mM KCl, 2 mM $MgCl_2$, 1 mM EDTA, 1 mM dithiothreitol, 10 mM potassium phosphate, pH 7.0 at 0°) at 4°C. Small pieces of muscle were then homogenized and centrifuged to remove nuclei and any remaining pieces of muscle. The quality of the myofibrils was checked repeatedly by phase microscopy during the procedure.

Myofibrils were stained for fluorescence analysis by spreading a drop of prepared isolated myofibrils on cold coverslips and fixing the myofibrils with 3.7% formalin (Sigma, St. Louis, MO) for 5 min at 4°C. Staining was performed as previously described (Almenar-Queralt et al., 1999b). α-actinin was localized by staining with a mouse monoclonal antibody EA53 (Sigma) at 1:750 for 45 min, followed by staining with a fluorescently-labeled anti-mouse secondary antibody (Jackson ImmunoResearch Laboratories, West Grove, PA) at 1:200 for 30 min. Tmod was localized with a rabbit polyclonal antibody (r3577) against chicken Sk-Tmod (Tmod4) at 1:500 for 45 min and with a fluorescently labeled anti-rabbit secondary antibody (Jackson ImmunoResearch Laboratories) at 1:200 for 30 min (Almenar-Queralt et al., 1999b). Bodipy-FL-phallacidin (Molecular Probes, Eugene, OR) was used at 1:200 for 30 min. Coverslips were washed for 30–45 min in phosphate-buffered saline between antibody steps.

Cultures of embryonic chick cardiac myocytes were prepared as previously described (Gregorio and Fowler, 1995; Littlefield et al., 2001). Tmod was localized with a mouse monoclonal antibody (mAb95) to chicken E-Tmod (Tmod1) at 2 μg/ml for 45 min and with an appropriate secondary antibody at 1:200 for 30 min (Almenar-Queralt et al., 1999a,b).

Microscopy

Myofibrils were examined by wide field epifluorescence on a Zeiss Axioskop with a 63× plan-apochromat lens (NA 1.40) (Zeiss, Hamburg, Germany). Based on the emission wavelength (~520 nm) and numerical aperture, the expected resolution for our images was 230 nm (0.61 * 520/1.4). Digital images were collected on a cooled 12-bit CCD camera with a Sony Interline 1300Y chip with 6.9 × 6.9 μm pixels (Roper Scientific, Trenton, NJ). The pixel size of the images was determined using a stage micrometer to be 0.1037 × 0.1037 μm, significantly smaller than the theoretical resolution of the microscope. Furthermore, the pixel size was also suitable for the thin filament lengths, Z line widths, and the fluorescence intensity of the myofibrils. Digital images of myofibrils were stored as 12-bit stacks in IP Lab (Scanalytics, Inc., Fairfax, VA).

For some experiments, images were collected on a Biorad 1024 confocal microscope with a 63× plan-apochromat lens (NA 1.40) (Zeiss). The pixel size was set to 0.100 μm using the zoom function. The pinhole was opened maximally to collect the most light and approximate wide field images *Z* axis position was moved at 0.12-μm intervals with a stepper motor attached to the fine focus controls. Each 8-bit image was Kalman averaged (five times) to reduce noise. Image series from three PM myofibrils stained for Tmod and α-actinin were converted and stored as 8-bit stacks in IP Lab. The origin of the *z* axis scale was chosen to coincide with the image determined to be most focused by visual inspection.

Image and Data Analysis

All myofibril images were reviewed before quantitation to ensure that the staining and the image focus were optimal. Line scans were determined for portions of myofibrils that were straight, contained five or more sarcomeres, and had striations relatively perpendicular to the long axis of the myofibril. In addition, the areas immediately above or below the myofibril region had to be suitable for background subtraction. Myofibrils meeting these criteria were easily found in isolated myofibril preparations and were present in cultured embryonic chick cardiac myocytes. Line scans were calculated using IP Lab and Microsoft Excel 98. First, the selected myofibril was oriented horizontally by computationally rotating the image stacks in IP Lab. Next, a rectangular region of interest typically 6–8 pixels wide was chosen along the selected myofibril (Fig. 2 *A*, *center box*) and the median intensity was determined in Excel as a function of position along the myofibril (Fig. 2 *B*, *M*). For background subtraction, two rectangular regions of interest typically 12 pixels wide were chosen above and below the myofibril (Fig. 2 *A*, *upper* and *lower boxes*) and the minimum intensities were determined in Excel for both background regions (Fig. 2 *B*, b_1 and b_2). Finally, the minimum intensity above and below the myofibril (minimum of b_1 and b_2) was subtracted from the median value (*M*) to determine the line scan intensities along the myofibril.

Line scans were modeled using Excel spreadsheets custom-designed for distributed deconvolution (available at www.scripps.edu/cb/fowler). The parameter values for the model were initially estimated by visual inspection. The Excel Solver add-in was used to refine the parameters through an interactive fitting procedure that minimized the error between the observed line scan intensities and the modeled intensities (Appendix, Eq. A10). After

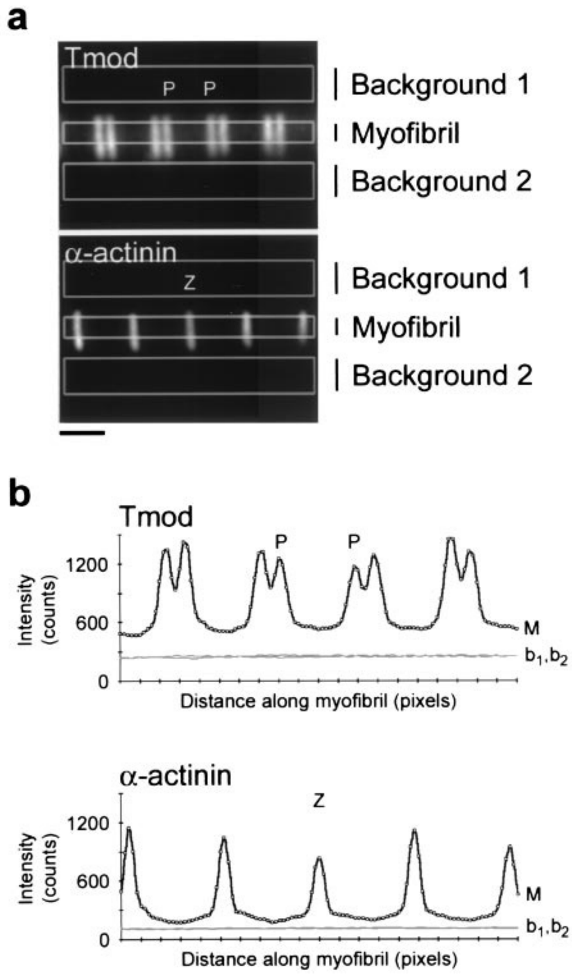

FIGURE 2 Quantitation of myofibril fluorescence. (*A*) Fluorescence micrographs of a striated chicken PM myofibril stained with Tmod to identify thin filament pointed ends (*P*) and α-actinin to identify Z lines (*Z*). Two background regions (*upper* and *lower boxes*) and a region through the myofibril (*center box*) are used to quantitate the fluorescence intensity along myofibrils. Bar = 2 μm. (*B*) Line scan quantitation of Tmod and α-actinin fluorescence intensity along myofibril from (*A*). The pointed ends of the thin filaments (*P*) and Z lines (*Z*) are visible in the Tmod and α-actinin line scans, respectively. *M*, median intensity from the region through the myofibril. b_1 and b_2, minimum intensities from the background regions above and below the myofibril, respectively. The line scan is the fluorescence intensity along the myofibril above the minimum background intensity.

a solution was determined for a myofibril line scan, the parameters for the solution were stored in a database for statistical analysis. Enhanced line scans were generated in Excel by reducing the Gaussian width parameter by 50%. Enhanced images were generated from these line scans using IP Lab and a text editor (Simple Text, Apple). Student T-tests were performed using the Excel analysis tools.

Because each fluorescent probe independently determines the positions of each Z line along the myofibril, the precision of the Z-line positions was determined for double-stained myofibrils by two methods. In the first method, it was assumed that any average displacement of the Z-line positions between the pair of line scans was due to an offset between the different fluorescent images (typically 1–2 pixels). Thus, the precision of the Z-line positions was considered to be equal to the standard deviation around this average displacement. In the second method, absolute differences in sarcomere lengths for the line scans were calculated from the Z-line positions. The precision of the Z-line positions was considered to be equal to the average absolute difference in sarcomere length. Both methods yielded similar results for each type of myofibril.

The jack-knife test randomly chooses a "working" data set containing 80% of the data points from the line scan to determine the model parameters and the calculated intensities. The remaining "test" data set, containing 20% of the data points were used to independently assess the goodness of fit. Jack-knife tests were repeated five times for each line scan to determine the statistical variation and the stability of each model. The average R free (average R factor of the test data set) and the variation in the parameters are reported in Table 2.

THE MODEL

Overview

Distributed deconvolution analysis models a line scan as a combination of three independent fluorescent intensity distribution functions: the "Gaussian distribution" function, the "Z-line distribution" function, and the "thin filament distribution" function (Fig. 3 *A*; Eq. A2). Briefly, the Gaussian distribution accounts for the spread of light at different focal positions, whereas the Z-line distribution accounts for sarcomere lengths and myofibril thickness. The thin filament distribution accounts for the location of thin filament components (e.g., phallacidin, Tmod, and α-actinin) within a thin filament array and is thus particularly important for determining thin filament lengths. Convolution of the thin filament and the Gaussian distribution functions generates the thin filament profile, whereas convolution of the thin filament profile with the Z-line distribution function generates the myofibril profile (Fig. 3 *A*). The thin filament profile and the myofibril profile correspond to a line scan of a single thin filament array and of a myofibril (i.e., a series of thin filament arrays), respectively. Unlike conventional deconvolution procedures using Fourier-based algorithms, distributed deconvolution uses an iterative fitting procedure to calculate the thin filament, Gaussian, and Z-line distribution functions and generates the myofibril profile that best approximates the observed myofibril line scan. Below, we first describe the Gaussian and Z-line distribution functions that are used to model all myofibril line scans. Finally, we describe the distribution functions specifically associated with phallacidin, Tmod, and α-actinin, including the thin filament distribution functions, the thin filament profiles, and the myofibril profiles.

The Gaussian distribution function

In wide-field microscopy, fluorescence is redistributed according to the three-dimensional (3D) point spread function (PSF) of the microscope, which results in blurring of a line scan along the myofibril (Agard et al., 1989). Furthermore, the degree of blurring is expected to vary depending on the

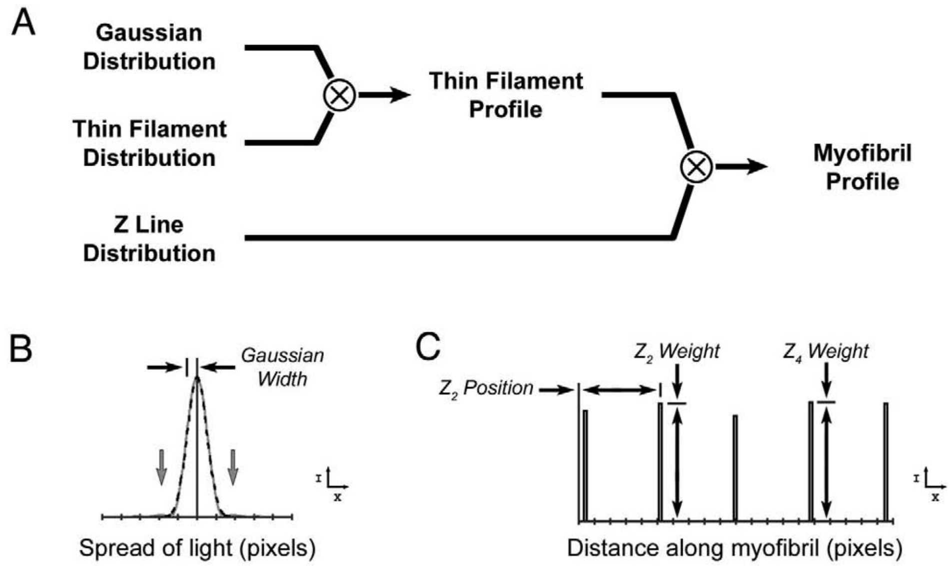

FIGURE 3 Schematic diagram of distributed deconvolution. (*A*) Three distribution functions are convoluted to generate the myofibril profile. The Gaussian and thin filament distribution functions are convoluted to generate the thin filament profile. The thin filament profile and Z-line distribution function are convoluted to generate the myofibril profile. (*B*) The Gaussian distribution function (*dotted black line*) is nearly superimposed on the theoretical PSF (*gray line*). The parameter *Gaussian width* determines the width of the Gaussian distribution. Gray arrows indicate the location of additional side peaks in the theoretical PSF. (*C*) The Z-line distribution function determines how thin filament profiles are organized into myofibrils. The Z-line distance parameters (e.g., Z_2 position) and Z-line weight parameters (e.g., Z_2 weight, Z_4 weight) determine the locations and relative intensities for each Z line. Axes in (*B*) and (*C*) indicate the direction of intensity (*I*) and position (*x*). The graphs in (*B*) and (*C*) are scaled separately.

position of the focal plane with respect to the myofibril (i.e., on the image focus). Distributed deconvolution approximates this variable blurring of the line scan with a one-dimensional (1D) Gaussian (normal) distribution function, which has a variable standard deviation (Gaussian width) (Fig. 3 *B*; Eq. A3). This distribution approximates the blurring of the microscope at different focal planes by varying the Gaussian width parameter. A Gaussian distribution with a large Gaussian width describes the spread of light from an unfocused myofibril image, whereas a Gaussian distribution with a small Gaussian width describes the spread of light from a focused myofibril image. Because a single value of Gaussian width is used for an entire myofibril line scan, the image should be at a constant focus along the length of the myofibril (i.e., parallel with the focal plane). Furthermore, because the Gaussian distribution has an area equal to one for all values of the Gaussian width parameter, the distribution function describes how the fluorescence from one pixel is distributed to its neighboring pixels. A myofibril line scan can be either restored to an ideal, unblurred distribution, i.e., deconvolved, by removing the Gaussian distribution completely, or computationally enhanced by replacing the experimentally determined Gaussian distribution with a Gaussian having a smaller Gaussian width.

A Gaussian distribution is a good approximation for the theoretical PSF for several reasons. Both distributions are symmetrical functions and are nearly superimpossible when the Gaussian width is approximately ⅓ of the distance to the first minimum in the PSF (i.e., the resolution of the microscope) (Fig. 3 *B*). Based on the 230-nm resolution of the microscopes we used for this study (see Methods), the corresponding Gaussian distribution would have a width of 0.7 pixels (~73 nm). However, this is the smallest width attainable and assumes that the source of light is a single point instead of two-dimensional disk (e.g., a Z line) and that no out-of-focus light contributes to the observed distribution. For a Gaussian with a width of 1.5 pixels, the average error is less than 3% up to 3 pixels away from the source. The largest difference is at the second peak of the PSF, however this accounts for less than 2% of the total fluorescence intensity. We chose to approximate the theoretical PSF of the microscope using a Gaussian distribution because the number of terms required to describe the single peak of the Gaussian distribution (Eq. A8b) was less than the number required for the multiple peaks of the theoretical PSF. The reduction in the number of terms increases the speed of the model. Furthermore, a Gaussian distribution could account simply for changes in focus and was particularly appropriate for the blurring that resulted from slightly oblique striations.

The Z line distribution function

The Z-line distribution function specifies the locations and relative intensities of the Z lines along the myofibril, thus describing the organization of thin filament arrays into

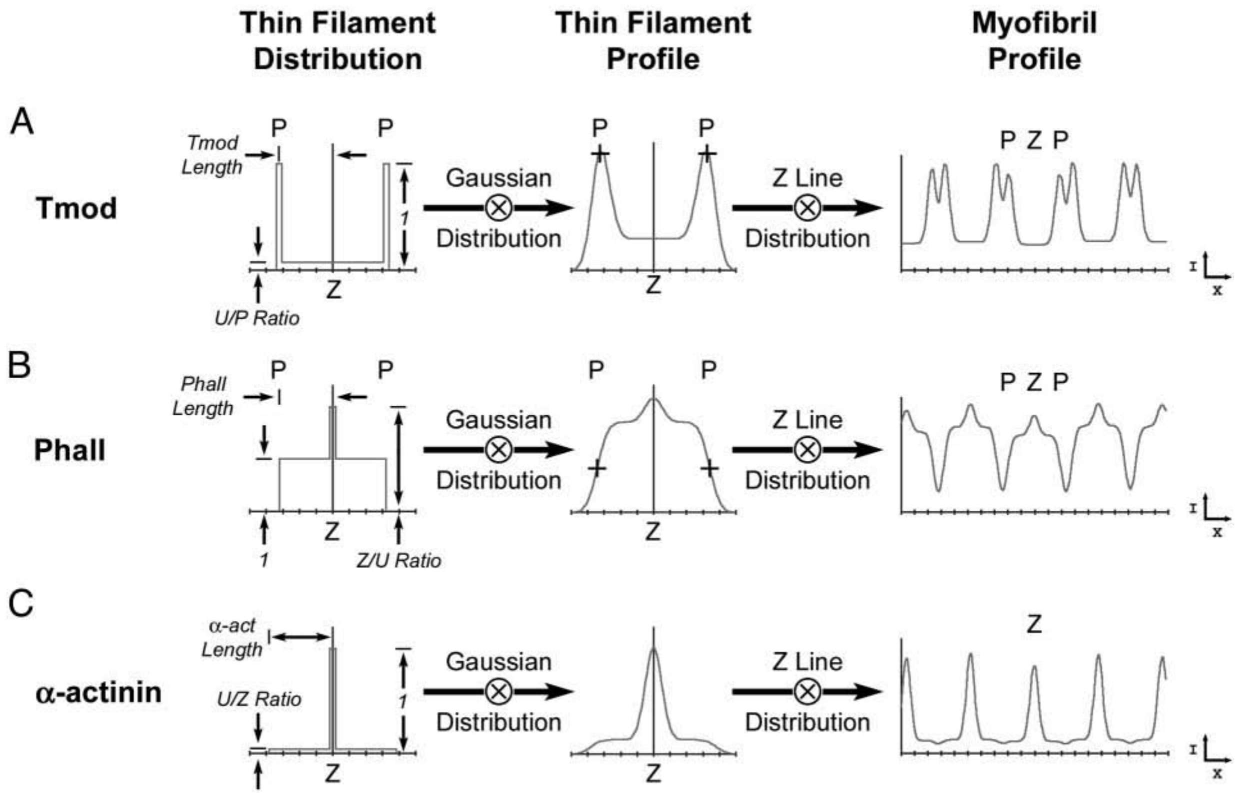

FIGURE 4 Thin filament distribution functions for Tmod, phallacidin, and α-actinin. (*left*) Thin filament distribution functions for (*A*) Tmod, (*B*) phallacidin, and (*C*) α-actinin. (*middle*) Thin filament profiles for (*A*) Tmod, (*B*) phallacidin, and (*C*) α-actinin after convolution with the Gaussian distribution. (*right*) Myofibril profiles for (*A*) Tmod, (*B*) phallacidin, and (*C*) α-actinin after convolution with the Z-line distribution. *P*, pointed ends; *Z*, Z line. Axes indicate the direction of intensity (*I*) and position (*x*) for all the graphs. Each graph is scaled separately for display.

myofibrils (Fig. 3 *C*). The Z-line distribution function is a 1D modified Dirac delta distribution, or "comb" distribution, that has two parameters for each Z line in the myofibril line scan: Z-line position and Z-line weight (Eq. A4). The Z-line positions determine where the Z lines are located along the myofibril line scan and the Z-line weights determine the overall intensities of the Z lines. Thus, for myofibril line scans with 10 Z lines, 20 parameters describe the position and intensities for all of the Z lines. The number of Z lines included in the model is determined from visual inspection of the myofibril image and includes any Z line within ~5 pixels from either end of the region chosen for the line scan. Sarcomere length (i.e., the distance between neighboring Z lines) is easily determined from the Z-line positions. The Z-line weights account for different relative Z-line intensities that may arise from variations in myofibril thickness. However, the Z-line weights are also dependent on the exposure time of the image and the fluorescent and biochemical properties of the probes used for localization. By normalizing the fluorescence from all the thin filament arrays, the Z-line distribution allows an average thin filament array to be determined from the entire line scan.

Thin filament distribution functions

The thin filament distribution functions describe the distribution of components in the thin filament array (Eq. A6). Because the thin filament array is symmetric on both sides of the Z line, the thin filament distribution functions are symmetric with the Z line located at the center and with the thin filament pointed ends located on both sides. Tmod, phallacidin, and α-actinin are each modeled with a different distribution function (Fig. 4). Each distribution function has two parameters and was selected based on the known location of the protein, the binding site for probes such as phallacidin, or the reactive epitope for antibodies. These distribution functions serve as basic examples; however, we have used additional distributions for other applications (Littlefield et al., 2001). The choice of the distribution function depends primarily on the component or feature of the myofibril that has been imaged.

Tropomodulin

The thin filament distribution function for Tmod is based on the location of Tmod at the thin filament pointed ends in striated muscle (Fowler et al., 1993; Almenar-Queralt et al., 1999b) (see Fig. 2 *A*). The Tmod distribution function consists of two peaks on both sides of the Z line and a low uniform fluorescence between the peaks (Fig. 4 *A*, *left*). The Tmod length parameter determines the location of the peaks with respect to the Z line (i.e., the middle of the distribution) and is expected to correspond to the length of the thin filaments. The U/P ratio parameter determines the uniform fluorescence intensity along the thin filament array relative to the peaks at the pointed ends. The uniform intensity was included based on visual inspection of Tmod line scans and was probably due to nonspecific antibody trapping along the myofibril. It served as an internal standard for the pointed-end staining intensity. The U/P ratio would be zero in an ideal situation where there was no background staining along the middle of the thin filament arrays.

The convolution of the Tmod distribution function with the Gaussian distribution results in the Tmod profile (Fig. 4 *A*, *middle*), which consists of two major peaks of fluorescence intensity at the ends of the thin filament array and low fluorescence in the middle of the array. This profile corresponds to the intensity from one thin filament array stained with Tmod. The pointed ends of the thin filaments, as determined by Tmod distance, are located at the center of the peaks. The convolution of the Tmod profile with the Z-line distribution results in the Tmod myofibril profile (Fig. 4 *A*, *right*), which corresponds to the line scan of a myofibril stained with Tmod.

Phallacidin

The thin filament distribution function for phallacidin staining is based on the known location of actin along the thin filaments, the overlap of thin filaments at the Z line, and the ability of phallacidin and phalloidin to bind uniformly along filaments in a 1:1 ratio with monomers (Squire, 1997; De La Cruz and Pollard, 1994; Cano et al., 1992) (see Fig. 5 *a*). Because there is an equal number of phallacidin binding sites along the free portion of the thin filament and additional sites at the Z line due to thin filament overlap, the phallacidin distribution function consists of a uniform distribution with an additional peak at the Z line (Fig. 4 *B*, *left*). The phallacidin length parameter determines how far the uniform distribution extends from the Z line, and is expected to be equal to the thin filament length. The Z/U ratio parameter is unitless and determines the relative intensity at the Z line with respect to the uniform intensity along the thin filament length. This ratio parameter is expected to be related to the width of the Z line, because wider Z lines would be expected to bind relatively more phallacidin with respect to the free portion of the thin filament (Eq. A14).

The convolution of the phallacidin distribution with the Gaussian distribution results in the phallacidin profile (Fig. 4 *B*, *middle*), which consists of a central peak with two shoulders. This profile corresponds to the intensity from one thin filament array stained with phallacidin. The pointed ends of the thin filaments, as determined by phallacidin length, are located at the half-maximal intensity on the shoulders. The convolution of the phallacidin profile with the Z-line distribution results in the phallacidin myofibril profile (Fig. 4 *B*, *right*), which corresponds to the line scan from a myofibril stained with phallacidin.

α-actinin

The thin filament distribution function for α-actinin staining is based on the specific localization of α-actinin to the Z line in myofibrils (Vigoreaux, 1994; Sanger et al., 1986; Dabiri et al., 1997). The α-actinin distribution function consists of a single peak of unitary fluorescence one pixel wide at the Z line and low background fluorescence along the length of the thin filaments (Fig. 4 *C*, *left*). The α-actinin length parameter determines how far the uniform fluorescence extends from the Z line and the U/Z ratio parameter determines its intensity relative to the peak at the Z line. The uniform, background intensity was included as an internal standard for the Z-line staining. In an ideal situation, when there was no background staining along the thin filaments, the U/Z ratio would be zero. Because any low uniform fluorescence probably results from nonspecific staining, the α-actinin length parameter is not related to thin filament length.

The convolution of the α-actinin distribution with the Gaussian distribution results in the α-actinin profile (Fig. 4 *C*, *middle*), which consists of a single peak with low background fluorescence. The profile represents how a single thin filament array would appear if stained for α-actinin. The convolution of the α-actinin profile with the Z-line distribution results in the α-actinin myofibril profile (Fig. 4 *C*, *right*), which corresponds to a line scan from a myofibril stained for α-actinin.

RESULTS

Evaluation of distributed deconvolution using chicken pectoralis major myofibrils

We stained isolated chicken pectoralis major (PM) myofibrils for Tmod and with phallacidin to determine the lengths of the thin filaments using distributed deconvolution. Within a preparation, individual myofibrils could be classified as being either stretched, relaxed, or hypercontracted according to their Tmod and phallacidin staining patterns. In stretched myofibrils, Tmod striations appeared as doublets that colocalized with gaps in the phallacidin staining (H zones), indicating that the pointed ends were separated in the middle of the sarcomeres (Fig. 5 *A*). In relaxed myofibrils, Tmod striations appeared as singlets because the thin filament pointed ends were located within the resolution limit of the microscope (see Methods) and only small H

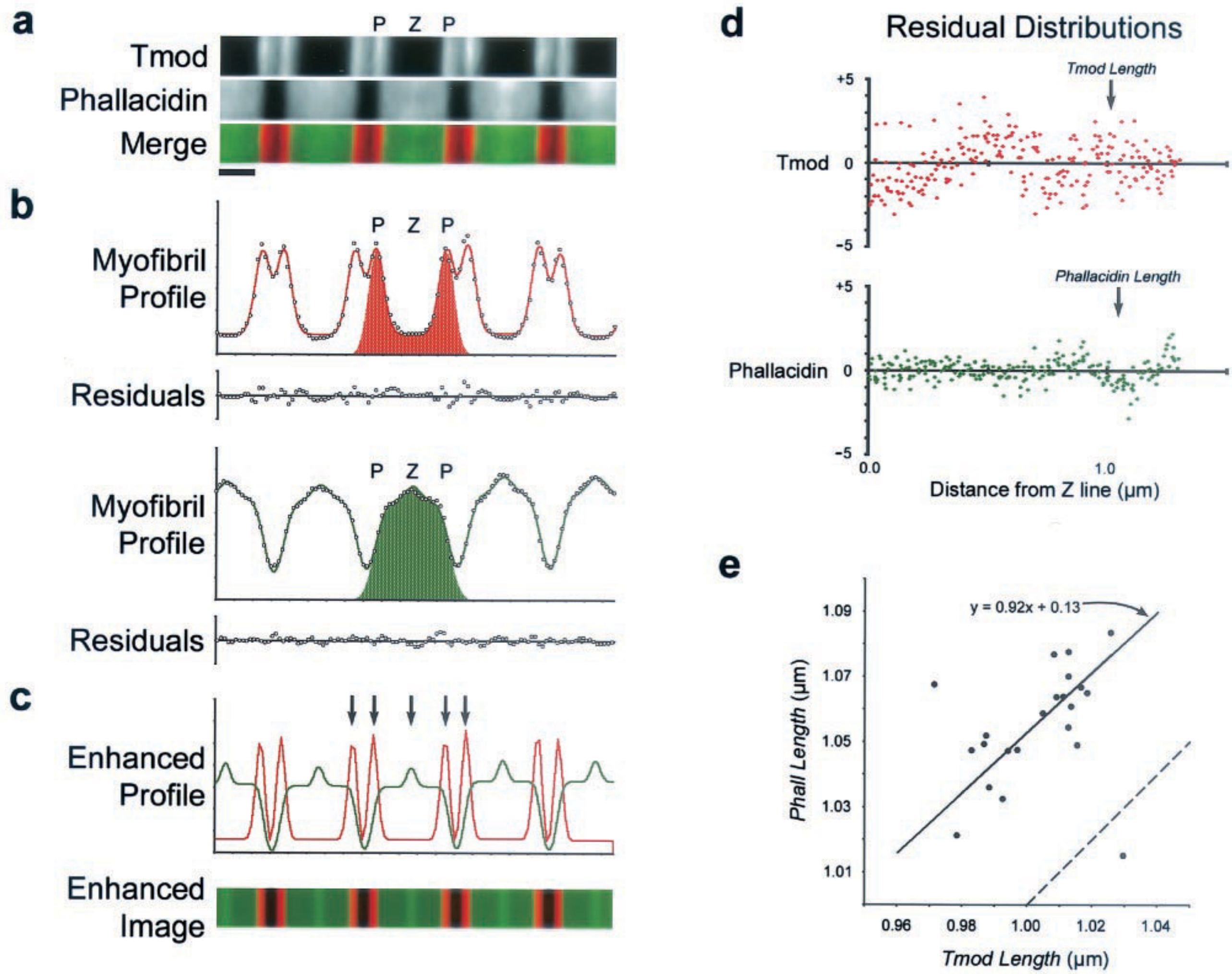

FIGURE 5 Thin filament lengths of chicken Pectoralis myofibrils are accurately determined by deconvolution of Tmod and phallacidin. (*A*) Isolated chicken pectoralis major myofibril images stained for Tmod and with phallacidin. Merge of Tmod (*red*) and phallacidin (*green*) images shows partial colocalization at pointed ends (*P*). Z lines (*Z*) are visible as bright bands by phallacidin staining. Scale bar is 1 μm. (*B*) Myofibril intensity profiles (*line*), line scan intensities (*circles*, *upper graph*), and residual data (*circles*, *lower graph*) for Tmod (*red*, *top*) and phallacidin (*green*, *bottom*). A thin filament profile is illustrated in each myofibril profile. (*C*) Enhanced line scans and corresponding image of Tmod (*red*) and phallacidin (*green*) staining generated by reducing Gaussian width parameters by 50%. Tmod doublets and phallacidin staining at Z lines are enhanced (*arrows*). (*D*) Normalized residual distributions for Tmod (*red*) and phallacidin (*green*). The lengths of the thin filaments as determined from Tmod and phallacidin are indicated. *Y* axis, normalized intensity (residual intensity/square-root of line scan intensity); *x* axis, distance from the Z line (μm). (*E*) Positive correlation between Tmod distance and phallacidin distance parameters. Each point represents one myofibril. *Solid line*, best fit trend line excluding two outliers. *Dashed line*, ideal line, $y = x$.

zones were visible by phallacidin staining (not shown). In hypercontracted myofibrils, Tmod striations appeared as doublets because of the extensive overlap of thin filament pointed ends from adjacent thin filament arrays. However, no H zones were visible by phallacidin staining (not shown). In addition, phallacidin stained ~5% of the myofibrils only near the barbed and pointed ends of the thin filaments and not along their length (not shown). This "end-staining" pattern of phallacidin staining has previously been observed for striated myofibrils and has been attributed to nebulin binding (Almenar-Queralt et al., 1999a; Zhukarev et al., 1997; Ao and Lehrer, 1995; Ojima et al., 1999; Bukatina et al., 1996).

For this investigation, stretched myofibrils were chosen for distributed deconvolution analysis because these types of myofibrils provided two independent measurements of thin filament length. We did not initially analyze relaxed, hypercontracted, or end-stained myofibrils because their patterns of Tmod and phallacidin fluorescence prevented dual-image analysis. For example, in relaxed myofibrils, it was unclear whether each Tmod striation could be unambiguously resolved into separate thin filament profiles. Con-

TABLE 1 Thin filament distribution parameters and modeling parameters determined by distributed deconvolution

Sample	Chicken PM	Chicken PLD	Cardiac Myocytes
Phallacidin			
Distance (μm)	1.055 ± 0.017	1.178 ± 0.042	0.795 ± 0.047
Z/U ratio	1.98 ± 0.19	2.59 ± 0.24	1.22 ± 0.64
Error (%)	2.13 ± 0.32	2.62 ± 0.59	2.51 ± 0.48
R-factor (%)	2.5 ± 0.4	3.7 ± 1.1	2.9 ± 0.6
Area (%)	100.3 ± 1.2	101.0 ± 2.8	99.9 ± 0.2
Tmod			
Distance (μm)	1.003 ± 0.015	1.110 ± 0.036	0.841 ± 0.062
U/P ratio	0.06 ± 0.01	0.07 ± 0.02	0.10 ± 0.05
Error (%)	3.93 ± 0.63	4.48 ± 1.01	3.88 ± 1.22
R-factor (%)	7.5 ± 1.6	8.0 ± 2.1	9.4 ± 3.0
Area (%)	100.2 ± 1.0	101.1 ± 3.0	99.7 ± 0.3
Number of Myofibrils	22	24	12
Average Sarcomeres/Myofibril	7.4 ± 1.4	6.1 ± 1.2	8.4 ± 1.8

versely, phallacidin staining could not be analyzed in hypercontracted myofibrils because there were no visible H zones. However, the thin filament lengths and staining parameters obtained for stretched myofibrils were representative of all types of myofibrils. For instance, when phallacidin staining was analyzed in relaxed myofibrils or when Tmod staining was analyzed in hypercontracted myofibrils, the thin filament lengths and intensity parameters were identical to those obtained from stretched myofibrils (not shown). These results supported previous observations that thin filament lengths do not change significantly during contraction (Sosa et al., 1994) and indicates that we have not biased our length measurements by selecting stretched myofibrils for analysis.

For each stretched myofibril, Tmod and phallacidin line scans were calculated (Fig. 5 *B*, *open circles*) and analyzed by distributed deconvolution using the Tmod and phallacidin distribution functions described in Fig. 4, *A* and *B* (Eq. A6). The myofibril profiles for Tmod and phallacidin (Fig. 5 *B*, *red* and *green lines*) were very similar to the observed line scans. In particular, the Tmod and phallacidin residuals did not show any trends along the myofibril (Fig. 5 *B*, *residuals*). Overall, the residuals were normally distributed about zero, which resulted in close agreement between the total fluorescence intensity (area) of the myofibril line scans and calculated profiles for Tmod (100.2 ± 1.0%) and phallacidin (100.3 ± 1.2%) (Table 1). In addition, the residuals for Tmod and phallacidin were similar for high- and low-intensity data, although, for some myofibrils, the Tmod residuals for low-intensity data were relatively large (not shown). Together, this indicated that each myofibril is composed of repeating Tmod and phallacidin profiles (e.g., Fig. 5 *B*, *shaded profiles*) and suggests that random noise in the image is the principal source of the differences between the observed and calculated intensities. For each myofibril, the Tmod and phallacidin residuals were used to determine R-factors, which measure the inaccuracy between the myofibril profile and line scan, such that a better model has a smaller R-factor (see Methods and Eq. A11). The R-factors were 7.5 ± 1.6% for Tmod and 2.5 ± 0.4% for phallacidin (22 myofibrils) (Table 1). These values suggested that distributed deconvolution accurately and reliably modeled the distribution of Tmod or phallacidin fluorescence in each entire PM myofibril with a single thin filament profile.

The Gaussian width parameters of the PM myofibrils were 2.04 ± 0.27 pixels for Tmod and 2.18 ± 0.25 pixels for phallacidin, indicating that the PM myofibril images were consistently well-focused. Furthermore, the Gaussian widths for Tmod and phallacidin were correlated (p = 0.016), consistent with each pair of myofibril images being acquired at the same focus. The values for the Gaussian width parameters were significantly higher than the theoretically attainable value of 0.7 pixels (see above), suggesting that the out-of-focus light and the cylindrical geometry of the myofibrils contributed significantly to the Gaussian distribution. Enhanced line scans and images generated using a Gaussian width parameter equal to 50% of the original value improved the appearance of Tmod doublets and the Z line staining by phallacidin (Fig. 5 *c*).

For the Z-line distributions, there was a strong correlation between the average sarcomere lengths determined from Tmod and phallacidin staining ($p = 2.1 \times 10^{-26}$), indicating that each probe accurately determined the location of the Z lines. In addition, the precision in the Z-line position parameters was 10 nm, as determined by directly comparing the locations of each Z line or the lengths of each sarcomere (see Methods). However, the median Z-line weight parameters were not strongly correlated for Tmod and phallacidin, suggesting that the relative brightness of Tmod and phallacidin staining were not directly dependent. Together, this data was consistent with the Gaussian distribution being determined primarily by the image focus, and with the Z-line distribution being determined by the actual distribution of Z lines in the myofibril.

The residuals from several PM myofibrils were analyzed according to their position with respect to the Z lines (Fig.

TABLE 2 Jack-knife analysis results for chicken PM myofibrils

Staining	Parameters	Myofibril 1	Myofibril 2	Myofibril 3	Myofibril 4	Myofibril 5
Tmod	R-factor (%)	6.0 (6.2)	6.5 (6.6)	5.9 (6.0)	10.3 (10.6)	5.9 (6.1)
	R free (%)	7.9	7.6	7.2	12.6	7.3
Phallacidin	R-factor (%)	2.7 (2.8)	2.5 (2.5)	2.1 (2.2)	2.8 (2.8)	2.4 (2.5)
	R free (%)	3.4	2.8	2.6	3.3	2.9
Tmod	Gaussian Width (pixels)	2.70 (2.71)	1.88 (1.88)	1.95 (1.96)	1.66 (1.65)	1.87 (1.87)
	Length (μm)	0.971 (0.971)	1.015 (1.015)	1.056 (1.024)	0.996 (0.997)	1.013 (1.013)
	P/U Ratio (%)	3.7 (3.8)	5.1 (5.1)	8.0 (7.8)	5.6 (5.6)	6.6 (6.6)
Phallacidin	Gaussian Width (pixels)	2.51 (2.51)	2.22 (2.22)	1.65 (1.65)	1.96 (1.96)	2.26 (2.26)
	Length (μm)	1.016 (1.016)	0.996 (0.997)	0.963 (0.963)	0.995 (0.995)	1.002 (1.002)
	Z/U Ratio	2.02 (2.02)	2.03 (2.04)	1.93 (1.93)	2.07 (2.07)	2.11 (2.11)

All values are expressed as Jack-knife result, average of 5 (original result).

5 *D*) to determine if any systematic errors in the models were correlated with the location of the Z lines. For this analysis, all residual values were normalized according to the square-root of the line scan intensity and plotted as a function of distance from the nearest Z line (see Methods). For Tmod, the variation (scatter) in the normalized residual values was maximal closer to the Z line (*red data points*). This was expected based on the low signal in that region. For phallacidin, slightly more variation was observed far from the Z line, in the middle of the H zone, where the phallacidin intensity also decreases (*green data points*). For both components, the residual values were approximately centered about zero for all positions along the thin filament array; however, the residuals would occasionally dip and rise around the axis. This trend may have resulted from slight differences between the Gaussian distribution function and the actual spread of light in the microscope. The residuals suggest that large inaccuracies are not present in the thin filament distributions.

The thin filament lengths determined from the Tmod and phallacidin thin filament distributions were very similar for all the PM myofibrils analyzed ($n = 22$; Table 1). For the phallacidin distribution, the phallacidin length was 1.055 ± 0.017 μm. For the Tmod distribution, the Tmod length was 1.003 ± 0.015 μm. Both of these lengths are in good agreement with previous determinations of thin filament lengths of PM myofibrils of 1.00–1.05 μm by electron microscopy (Page and Huxley, 1963; Ohtsuki, 1979; Kruger et al., 1991). The 15- and 17-nm standard deviation in Tmod length and phallacidin length, respectively, suggested that measurement of thin filament lengths by distributed deconvolution was very precise. In addition, Tmod length and phallacidin length parameters were correlated ($p = 1.9 \times 10^{-5}$) and exhibited a linear trend ($y = 0.92x + 0.13$) which was close to ideal ($y = x$) after two outliers were excluded (Fig. 5 *E*). This trend suggested that thin filament lengths varied ~40 nm between different individual PM myofibrils. However, the Tmod length parameters were 53 ± 9 nm less than the phallacidin length parameters, suggesting that a systematic error was present (compare solid to dashed line in Fig. 5 *E*). One possibility is that the difference between the Gaussian distribution and the microscope's PSF could result in misidentification of the extent of phallacidin staining at the pointed ends, thus leading to this discrepancy. Nevertheless, the Tmod length and phallacidin length parameters deviated only ~10 nm around this trend line, suggesting that the high precision of distributed deconvolution enabled small variations in PM thin filament lengths between different myofibrils to be detected.

The Z/U ratio was 1.98 ± 0.19 for phallacidin, consistent with additional Z-line staining from thin filament overlap at the Z line. This Z/U ratio corresponds to a Z-line width of 102 ± 20 nm, which is consistent with an ~100-nm Z-line width estimated from electron microscopy images in Kruger et al. (1991). The U/P ratio for Tmod was 5.6 ± 1.2%, indicating that the fluorescence intensity along the length of the thin filaments was only ~6% of the intensity at the pointed ends. This fluorescence was likely due to weak, nonspecific antibody binding (Gregorio and Fowler, 1995; Fowler et al., 1993).

The goodness of fit and the stability of particular models was determined using a modified jack-knife test on five pairs of Tmod and phallacidin line scans (see Methods). The jack-knife tests indicated that the models fit very well to the line scans and were very stable. The R-free values, which correspond to R factors (see Methods), were only slightly higher than the R factors determined for the "working" data set or for the entire data set (Table 2). This indicates that the model determined by distributed deconvolution was capable of accurately predicting the intensities along a myofibril using only a partial data set. The model was also very stable because the thin filament distribution parameters (Tmod distance, P/U ratio, phallacidin distance, and Z/U ratio) were generally accurate to within 1% of their original values and, in some cases, within 0.1% (Table 2). In addition, the values for Gaussian width were within 0.2–2.3% of their original values, the values for Z-line weight were within 0.5% of their original values, and the values for Z-line position were on average within 0.2–0.4 nm of their original values. This analysis suggests that some of the variations observed among PM myofibrils reflect real differences in

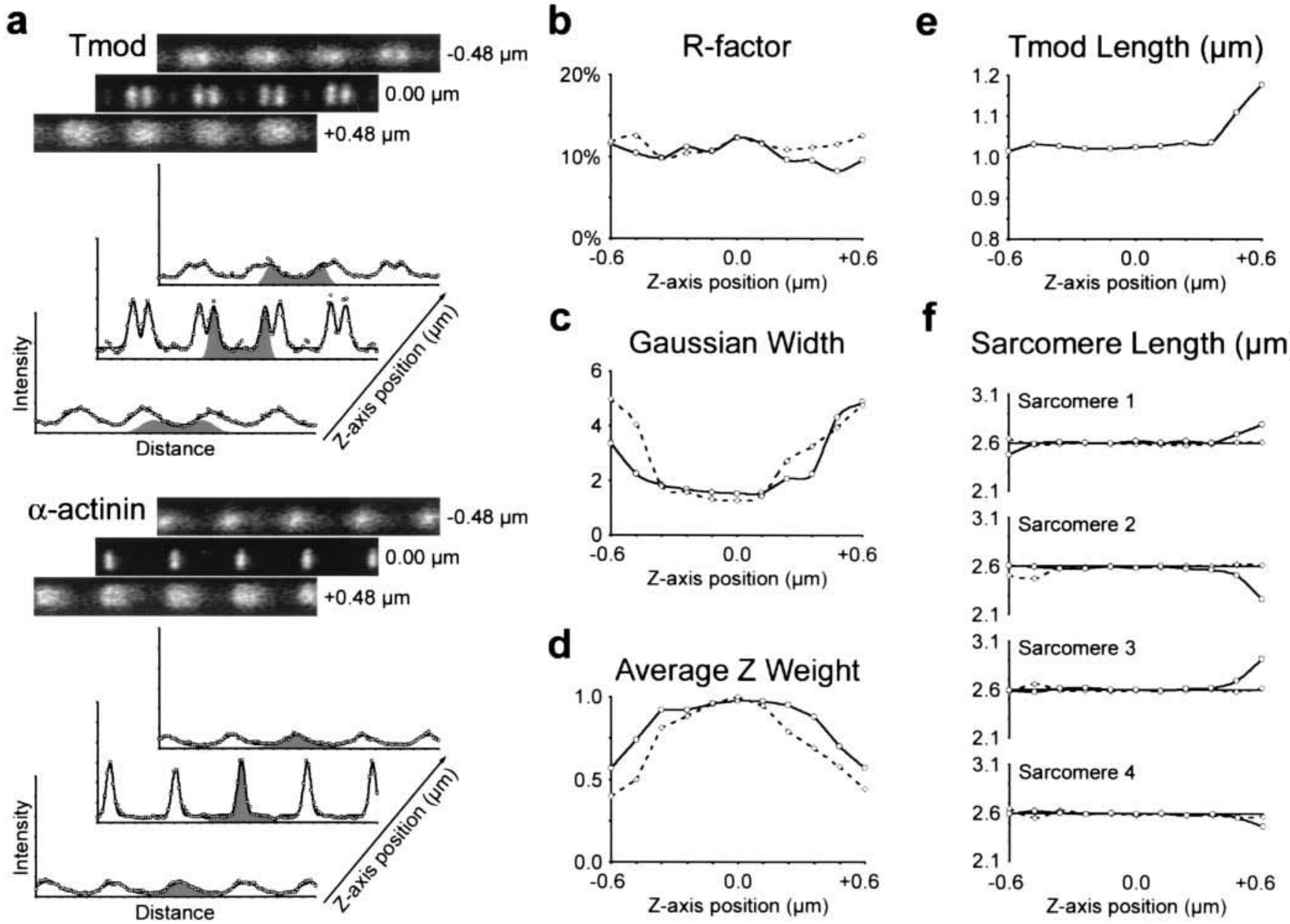

FIGURE 6 Thin filament lengths are accurately determined for myofibrils over a broad range of focus. (*A*) Images, line scans (*circles*), and intensity profiles (*lines*) for Tmod (*top*) and α-actinin (*bottom*) in chicken PM myofibrils from three focal planes (*z* axis positions $+0.48$, 0.00, and -0.48 μm). A thin filament profile is indicated for each myofibril intensity profile. All graphs are on the same scale. Dependence of (*B*) Gaussian width, (*C*) normalized average Z weight, (*D*) correlation coefficient for model, (*E*) Tmod length parameter, (*F*) and sarcomere lengths on focus (*z* axis position) for Tmod (*solid line*) and α-actinin (*dashed line*).

the organization of thin filament arrays and are not due to inherent imprecision in the models.

The effect of image focus on model parameters

To directly test the effects of image focus on the model, through-focus image series of single myofibrils were acquired on a microscope equipped with a *z*-axis stepper motor (see Methods). Through-focus series of phallacidin-stained myofibrils could not be analyzed by distributed deconvolution because phallacidin line scans were relatively uniform and featureless for defocused images. Instead, we used myofibrils stained for Tmod and α-actinin because their line scans have large modulations in fluorescence intensity over a wide range of focus. In Fig. 6 *A*, images of Tmod and α-actinin staining are shown for a single myofibril at three different focal planes ($Z = +0.48$, 0.00, and -0.48 μm). When the myofibril is in focus ($Z =$ 0.00 μm), the α-actinin peaks at the Z lines are sharp and the Tmod doublets are easily resolved. However, when the myofibril is out of focus ($Z = +0.48$ and -0.48 μm), the α-actinin peaks are blurry and the Tmod doublets are barely distinguishable. In addition to becoming blurred, the overall fluorescence intensity of the myofibril decreased as the myofibril was defocused (Fig. 6 *A*, compare line scans). Line scans for each Tmod and α-actinin image of the through-focus series was calculated and analyzed by distributed deconvolution (Fig. 6 *A*). The effect of focus on Gaussian width, Tmod distance, and sarcomere length was then determined as a function of *z*-axis position using the solutions to the model.

The Tmod and α-actinin distribution functions (Fig. 4, *A* and *C*) were used to model the line scans of Tmod and α-actinin staining at all focal planes. As usual, while solving for the best-fit model, both Tmod length and U/P ratio parameters in the Tmod distribution function were allowed to vary for each image in the focus series. The myofibril profiles for Tmod (Fig. 6 *A*; *top*, *solid lines*) approximated the line scans for all focal planes. The R factors for Tmod were 10.4 ± 1.2% and remained uniform for the entire focus series (Fig. 6 *B*, *solid line*). The larger R factors for Tmod were probably due to the increased noise in the 8-bit confocal image used for this experiment as compared to the 12-bit CCD images described previously. This indicated that this general Tmod distribution function (i.e., having two variable parameters; Fig. 4 *A*) could accurately model line scans in the focal series.

In contrast to the Tmod distribution function, the α-actinin distribution function was too general for modeling all the line scans in the focal series. Thus, when both α-actinin distribution function parameters (α-actinin length and U/Z ratio) were allowed to vary while solving for the best-fit model, the resulting α-actinin distributions for defocused images in the series were inconsistent with its known distribution at the Z line (data not shown). Alternatively, when the U/Z ratio was set equal to zero and not included as a variable, the background fluorescence in the focused images was not accounted for by the model and resulted in large R factors (~35%) (data not shown). However, the entire focus series was accurately modeled using a limited distribution function where the U/Z ratio was determined for one focused image ($Z = 0.00$), and subsequently held constant for all the other images (Fig. 6 *A*, *bottom*, *solid lines*). For this scenario, the R factors were 11.2 ± 1.2% and remained uniform for the entire focus series (Fig. 6 *B*, *dashed line*). This indicated that an α-actinin distribution function with a constant (but nonzero) background could accurately model the entire focus series.

As a myofibril was defocused, the values for Gaussian width parameters increased while the Z-line weight parameters decreased for both Tmod and α-actinin myofibril profiles (Fig. 6 *C*). In the most focused images ($Z = -0.24$ to 0.24 μm), the values of the Gaussian width were lowest and changed only slightly. In this region, the Gaussian width was ~1.8 ± 0.1 pixels for Tmod line scans and 1.5 ± 0.1 pixels for α-actinin ($n = 5$ positions). As the myofibril defocused, the Gaussian width generally increased by the same extent for both Tmod and α-actinin (Fig. 6 *C*). In contrast, when the α-actinin U/Z ratio parameter had been set to zero, the Gaussian width increased more for α-actinin than for Tmod as the myofibril was defocused (data not shown). Thus, there was a narrow range of focus that showed only slight effects on the Gaussian width value, but, on either side, the Gaussian width value was extremely dependent on focus. The average values of the normalized Z-weight parameters decreased as the myofibril was defocused (Fig. 6 *D*). Both Tmod and α-actinin Z-weight parameters decreased in parallel and were independent of the exact α-actinin distribution used. This decrease in fluorescence intensity was expected because the myofibril had steadily moved out of the focal plane.

In contrast to Gaussian width and Z-line weight parameters, which were dependent on focus, the thin filament lengths and the Z-line positions were generally independent of focus. For the representative myofibril shown in Fig. 6, the Tmod length parameter was 1.026 ± 0.006 μm over a 1.0-μm range of focus (Fig. 6 *E*). In general, the Tmod length remained constant over a 1.0–1.5-μm range of focus for different myofibrils. When the myofibril was further defocused, the deconvolution procedure did not accurately determine the length of the thin filaments (Fig. 6 *E*, $Z = +0.48$, $+0.60$ μm). At this distance, Tmod doublets were barely visible (Fig. 6 *A*, $Z = +0.48$ μm). Similar to the Tmod length parameter, the sarcomere lengths were accurately determined over the entire middle range of the focus series, and were less accurately determined when the myofibril was far out of focus (Fig. 6 *F*). The length of the sarcomeres ranged from 2.5 to 2.8 μm along the myofibrils analyzed, and the average variation over the five best-focused images was between 6 and 11 nm. Because the sarcomere length is reproduced accurately over a broad range of *z*-axis position, we conclude that the values for the Z-line position parameters are also accurately determined over a broad range of focus.

Application of distributed deconvolution to other myofibrils

To further investigate whether the variation in thin filament lengths observed for PM myofibrils also occurred for other myofibrils, we applied distributed deconvolution to chicken PLD myofibrils and to embryonic chick cardiac myocytes. Similar to PM myofibrils, PLD myofibrils and cardiac myocytes were stained for Tmod and for actin with phallacidin, and stretched regions were chosen to provide two independent measurements of thin filament length. The R factors for PLD myofibrils were 8.0 ± 2.1% for Tmod and 3.7 ± 1.1% for phallacidin (24 myofibrils); and, for cardiac myofibrils were 9.5 ± 2.9% for Tmod and 2.9 ± 0.6% for phallacidin (12 myofibrils) (Table 1). These were similar to the R factors for PM myofibrils and indicated that distributed deconvolution accurately reproduced the myofibril line scans for PLD and cardiac myocytes.

The thin filament lengths determined for PLD and cardiac myocytes were distinct from the PM lengths (Table 1). For PLD myofibrils, the phallacidin length parameters (1.178 ± 0.042 μm) were similar to the Tmod length parameters (1.110 ± 0.036 μm), indicating that the PLD thin filaments were ~1.1 μm in length. The lengths were slightly longer than previously reported values determined by EM (1.06 ± 0.04 μm), but were consistent with the range in filament lengths obtained (Kruger et al., 1991). Similarly, for cardiac myofibrils, the phallacidin length parameters (0.795 ± 0.047 μm) were similar to the Tmod length parameters (0.841 ± 0.062 μm), indicating that the cardiac thin filaments were ~0.8 μm in length. Together with PM myofi-

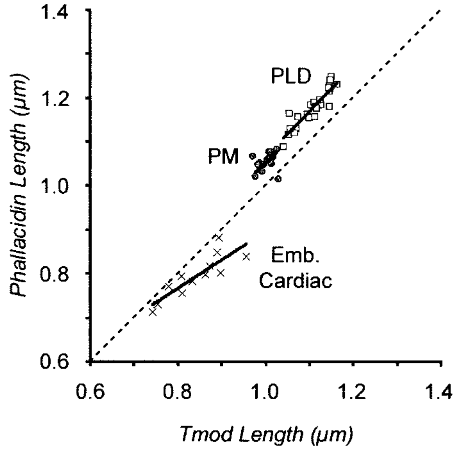

FIGURE 7 Correlation of thin filament lengths for adult PM (*gray circles*), adult PLD (*open squares*), and embryonic cardiac myocyte (×) myofibrils using Tmod and phallacidin fluorescence. *Solid lines*, best-fit trend lines for each muscle type. *Dashed line*, ideal line, $y = x$. PM data replotted from Fig. 5 *D*.

brils, these myofibrils give a wide range of thin filament lengths in which to compare Tmod and phallacidin staining.

Comparison of the Tmod and phallacidin length measurements indicated that there was significant variation in PLD thin filament lengths between myofibrils (Fig. 7, *open squares*). The Tmod length and phallacidin length parameters were closely correlated for PLD myofibrils ($p < 1 \times 10^{-9}$) and exhibited a linear trend ($y = 1.04x + 0.02$), which was close to ideal ($y = x$; Fig. 7, *dashed line*). The ~100-nm variation along this trend for PLD thin filaments was large compared to PM myofibrils (~40 nm) and indicated that PLD thin filament lengths could vary 10% or more. However, the position of the trend line above ideal was similar to PM myofibrils and suggested that modeling of phallacidin staining resulted in an ~50-nm overestimation in PLD thin filament lengths. Similar to PM myofibrils, the scatter in the Tmod length and phallacidin length values away from this trend line suggested that the precision of the thin filament length measurements was 10 nm or less for PLD myofibrils. Thus, distributed deconvolution was able to detect differences in average thin filament lengths and distinct variations in lengths between PM and PLD thin filaments despite the similar systematic and random errors associated with their measurement (Fig. 7, compare gray circles and open squares).

Similar to PLD and PM myofibrils, the cardiac thin filament lengths appeared to vary among different myofibrils; however, the relationship between Tmod length and phallacidin length parameters was less clear (Fig. 7, ×). Although these parameters were also correlated for cardiac myofibrils ($p < 1 \times 10^{-4}$), the trend line for the cardiac myofibrils ($y = 0.65x + 0.25$) deviated significantly from ideal ($y = x$; Fig. 7, *dashed line*). The correlation between Tmod lengths and phallacidin lengths suggested that cardiac thin filaments vary by as much as 100 nm in length, similar to PLD myofibrils. The position of the trend line below ideal suggested that cardiac thin filament lengths were underestimated by ~50 nm using phallacidin staining. This systematic underestimation in phallacidin length for the cardiac myofibrils was distinct from the overestimation observed for PM and PLD myofibrils and may have resulted from reduced phallacidin binding to thin filament ends (see below). Furthermore, the filament length measurements deviated from the trend line significantly more for cardiac than for PLD or PM myofibrils. The reduced precision of the method for cardiac myofibrils may result from their complex organization within the myocytes. Together, these differences suggested that there were different or additional sources of error associated with modeling of cardiac myofibrils than with PM and PLD myofibrils.

In addition to the thin filament length measurements, distributed deconvolution also determined the relative intensities of phallacidin and Tmod fluorescence along the thin filament array (Table 1, Z/U ratio and U/P ratio). For PLD myofibrils, the Z/U ratio for phallacidin was 2.59 ± 0.24, which suggested that the Z-line width for PLD was 165 ± 25 nm (~1.6 pixels). This width would be consistent with the ~140-nm Z-line widths we estimated from electron microscopy images of PLD in Kruger et al. (1991). For cardiac myofibrils, the Z/U ratio was 1.22 ± 0.64, which implied a cardiac Z-line width of ~23 ± 66 nm. This Z-line width was inconsistent with the ~110-nm Z-line widths estimated from electron microscopy images (Gregorio and Fowler, 1995; Lu et al., 1992). However, consistent with previous measurements, the maximum Z/U ratio for cardiac myocytes was 2.35, implying a maximum Z-line width of ~140 nm. Visual inspection of images also revealed variable and relatively weak phallacidin staining at the Z line. This suggested that less phallacidin bound to the cardiac thin filaments at the Z lines (i.e., at the barbed ends) than along the free portion, consistent with the unexpectedly low Z/U ratio.

Tmod staining for the PLD and cardiac myofibrils was similar to the PM myofibrils. The U/P ratio for Tmod was 0.071 ± 0.022 for PLD myofibrils and 0.100 ± 0.050 for cardiac myofibrils. This indicated that the background fluorescence was 7% and 10% of the peak intensity at the pointed ends for PLD and cardiac myofibrils, respectively. This was similar to the 6% background for Tmod staining in PM myofibrils. The slightly higher U/P ratio for cardiac myofibrils may reflect experimental (e.g., staining, extraction) or biological (e.g., isoform, solubility) differences between these myofibril preparations (Fowler et al., 1993; Gregorio and Fowler, 1995; Almenar-Queralt et al., 1999b).

DISCUSSION

Distributed deconvolution analysis restores and enhances myofibril line scans to determine the location and intensities of the fluorescence in the original image, and therefore, the actual distribution of components within the myofibril. We show that the method allows for quantitative comparison between different myofibrils by accounting for variations in focus and in sarcomere length. Using several statistical and experimental analyses, we show that the method accurately determines the lengths of thin filaments in isolated chicken myofibrils and embryonic chick cardiac myocytes with a precision up to 10 nm. The lengths of the chicken PM thin filaments determined here agree well with the lengths determined using electron microscopy by Ohtsuki (1979), Page and Huxley (1963), and Kruger et al. (1991). In addition, using independent probes, we show that thin filament lengths vary ~5% between different PM myofibrils and ~10% between different myofibrils in PLD and in embryonic cardiac myocytes. Distributed deconvolution serves as a bridge between electron- and light-microscopy techniques. The method has significant advantages and few limitations compared with these conventional techniques.

Merits of distributed deconvolution

The main strength of distributed deconvolution is the thin filament distribution function, which serves as an intermediate step between the whole myofibril and the individual point source of light. The ability to specify different thin filament distributions gives the method the flexibility needed to model the distribution of different thin filament components or processes. Here, we used three separate functions to describe phallacidin, Tmod, and α-actinin distributions. Previously, we used another distribution function to quantitate the initial incorporation of rhodamine-actin at the barbed and pointed ends of thin filaments (Littlefield et al., 2001). After a thin filament distribution function is specified, it places constraints on the fluorescence based on the structure and organization of thin filaments within the myofibril. For example, the thin filament distributions we used are two-fold symmetric based on the symmetry of the thin filament arrays in the myofibril (see Fig. 1). Similarly, because the thin filaments are composed of repeating actin subunits and because the phallacidin staining appeared uniform, we used a continuous thin filament distribution to model phallacidin. Finally, the thin filament distribution function allows different myofibrils to be compared quantitatively, independent of their thickness, their sarcomere lengths, and the focus of their images.

Several statistical analyses indicated that distributed deconvolution analysis is extremely precise at measuring lengths and distances. First, the precision in Z-line positions was 10 nm for PM, 20 nm for PLD, and 70 nm for cardiac myofibrils. The precision in the thin filament lengths was 9 nm for PM, 17 nm for PLD, and 50 nm for cardiac myofibrils. Second, Z-line positions and thin filament lengths for PM myofibrils were accurate over a wide range of focus, and the jack-knife results indicated that the Z-line positions and thin filament lengths were precise and stable. Together, they suggest that the Z-line positions and the thin filament lengths could be determined within 10–20 nm (0.1–0.2 pixels) under optimal conditions. This precision was possible because the entire thin filament profile was used to specify the position of the Z lines and the thin filament lengths (Gelles et al., 1988). Furthermore, the stability in the measurements for PM myofibrils indicates that the thin filament arrays are very similar to each other within a single myofibril.

Comparison of distributed deconvolution to other methods

There are two basic types of conventional deconvolution methods that use Fourier-based algorithms for image enhancement and restoration. At one extreme, an average or canonical molecular structure is determined from a repetitive array or lattice of identical molecules or subunits using classic Fourier methods (e.g., x-ray crystallography, helical reconstruction, etc.). This approach requires nearly identical structures to be organized in a regular array. However, many myofibrils are nonuniform and have a variety of sarcomere lengths and Z-line intensities, precluding this type of analysis (Littlefield et al., 2001). At the other extreme, conventional deconvolution microscopy uses Fourier techniques to remove defocused light and restore an image back to an ideal image based on the 3D spread of light from a single point source (i.e., the PSF). This approach does not make assumptions about the nature of the object being imaged. However, it is very sensitive to noise, and artifacts are easily generated in the reconstructed image (Zhukarev et al., 1997). Although distributed deconvolution uses line-fitting algorithms to deconvolve the component functions of myofibril line scans, the method combines aspects of both conventional approaches because myofibrils are simultaneously repetitive (e.g., thin filament arrays) and irregular (variable sarcomere lengths). Thus, distributed deconvolution independently determines the position and intensities of each thin filament array similar to conventional deconvolution microscopy, yet it uses reasonable constraints based on the repeating structure of myofibrils to determine an average (canonical) thin filament array similar to classic Fourier methods.

Distributed deconvolution also has significant advantages over Fourier methods because it directly models the overlap of fluorescence from adjacent thin filament profiles. This is particularly important for determining thin filament lengths because Tmod and phallacidin fluorescence from adjacent thin filament arrays overlap significantly even in relatively stretched myofibrils. Furthermore, because sarcomere lengths in vivo are relatively short compared to stretched, isolated myofibrils, distributed deconvolution can analyze living myofibrils in a physiologically relevant environment. In contrast, Fourier methods would be unable to account for the overlap between adjacent thin filament arrays and could not measure thin filament lengths directly.

Distributed deconvolution overcomes many limitations of electron microscopy methods because it uses fluorescence, which is specific, rapid, and noninvasive. The specificity of fluorescence probes allows the distributions of multiple, specific thin filament components to be determined. One of the difficulties in determining thin filament length from EM is deciding where the filament terminates. We used both phallacidin and Tmod fluorescence to provide two independent measurements of thin filament lengths for each myofibril. Furthermore, each probe independently determines the positions of each Z line along the myofibril, ensuring that they are identified precisely. In contrast, it is difficult to determine the location of specific thin filament components by electron microscopy because immuno-gold labeling is usually incomplete, does not efficiently penetrate into the A-I overlap region, and is difficult to quantitate (Kouchi et al., 1993). Although negative staining has been used to visualize stripes of troponin antibodies in isolated thin filament arrays, this procedure removes the thin filament arrays from their in situ context within an intact myofibril (Ohtsuki, 1979). Furthermore, because fluorescence can be detected quickly and is noninvasive, distributed deconvolution is capable of analyzing the distribution of myofibril components in living cells or unfixed samples (Littlefield et al., 2001).

Phallacidin and tropomodulin probes

Phallacidin staining may not be as reliable as Tmod for measuring thin filament lengths. One reason for this is the dependence of the phallacidin distribution function on the function chosen to describe how a point source of fluorescence is distributed in the microscope (i.e., the Gaussian distribution). Because phallacidin binds uniformly along the lengths of the thin filaments, any difference between the Gaussian distribution and the actual PSF of the microscope may be reinforced and magnified and result in significant deviations in length measurements. In contrast, the Tmod fluorescence distribution consists mainly of individual peaks at the pointed ends. Their location is primarily determined by the center of the peak, which is expected to be less sensitive to deviations between the Gaussian distribution and actual PSF.

Phallacidin may also be less useful than Tmod staining because of limitations in the distributed deconvolution method. In particular, phallacidin line scans can be relatively featureless depending on the focus of the image and the lengths of the sarcomeres. In contrast, Tmod staining at pointed ends results in line scans that have large intensity modulations over a wide range of focus. In addition, Tmod staining can be used to determine thin filament lengths with high accuracy in hypercontracted myofibrils (which have no H zones), and with moderate accuracy in relaxed myofibrils (not shown). This sensitivity in sarcomere lengths and image focus suggests that thin filament lengths may be determined accurately using phallacidin staining only in limited conditions.

Phallacidin may also be unreliable because it may not bind uniformly along the lengths of the thin filaments under all conditions. Indeed, a small proportion of the PM and PLD myofibrils were observed to stain with phallacidin only near their thin filament barbed and pointed ends. This variable binding may result in inaccurate measurement of Z-line width and thin filament lengths. Phallacidin staining appeared to be reduced at the Z line in cardiac myofibrils, leading to underestimations in Z-line width and perhaps in thin filament length. However, under ideal, saturating conditions, quantitative analysis of phallacidin binding to the Z line by distributed deconvolution may provide reasonable estimates of Z-line widths.

Despite the possible inaccuracy in absolute thin filament lengths, phallacidin fluorescence can still be used as a reliable probe for measuring relative differences in thin filament lengths. In particular, the phallacidin and Tmod lengths for PM and PLD myofibrils are correlated although they appear to be offset by a systematic error. Thus, myofibrils that stain further away from the Z line with Tmod also stain further away with phallacidin. We interpret this discrepancy in isolated myofibrils as an ~5% overestimation in thin filament lengths from phallacidin staining. However, this systematic overestimation still allows phallacidin staining to be used to determine relative thin filament lengths between myofibrils from different muscles.

Thin filament lengths

Using distributed deconvolution, we detected a moderate ~40-nm range in thin filament lengths in the chicken PM myofibrils and a more extensive ~100-nm range in chicken PLD myofibrils and embryonic chick cardiac myocytes. This variation was apparent from the correlation between Tmod length and phallacidin length parameters. This correlation would not have occurred if length variations for either Tmod or phallacidin resulted from random noise in the length measurements. Furthermore, differences in image focus for different myofibrils cannot account for the variation because Tmod length was accurately determined over a wide range of focus. The variations in thin filament lengths that we observe are unlikely to result from a fixation artifact because the treatment we used was mild. Furthermore, we observed evidence of similar variations in thin filament lengths in live cardiac myocytes (Littlefield et al., 2001). Together, our measurements indicate that thin filament lengths can vary between different myofibrils from the same muscle. This suggests that thin filament lengths may not be specified to a set length in vivo for a particular muscle and implies that a ruler molecule, such as nebulin, does not solely specify thin filament length. Instead, we have suggested that thin filament lengths may be specified primarily within the context of the entire myofibril to ensure that the thick and thin filaments overlap completely and produce maximal force (Littlefield and Fowler, 1998). Thus, slight differences in average sarcomere lengths in different muscle fibers may "tune" the lengths of the thin filaments to provide maximal thick and thin filament interactions. In continuously active muscles, such as cardiac muscle, the incessant changes in sarcomere length could result in relatively extreme variations in thin filament lengths, even within individual thin filament arrays, as previously observed (Robinson and Winegrad, 1979). Because the thin filament distribution models used here did not account for this possibility, it was not possible to quantify the extent of this variation.

Future applications

One improvement to distributed deconvolution would be the empirical determination of the 1D PSF to replace the estimated Gaussian distribution function. It may be possible to determine the PSF by acquiring focus series of myofibrils stained with α-actinin. In addition, it may be possible to adapt distributed deconvolution to 3D data sets to be used in conjunction with a 3D PSF. This would make the model independent from focus because all image planes would be collected and analyzed together, similar to conventional 3D deconvolution microscopy (Agard et al., 1989). However, the method would still have an advantage because it would still use a thin filament distribution function that could specify particular constraints based on the myofibril structure. Additionally, it would be possible to specify thin filament distribution functions that could measure thin filament lengths or relative intensities in the middle or at the edge of the myofibril. Considering that 3D deconvolution microscopes are readily available, this modification of the method would only require new software to work with the 3D data sets.

The method can also be improved by modeling the distribution of two or more probes (such as Tmod and phallacidin or Tmod and α-actinin) at the same time using common parameters for the Z-line and Gaussian distribution functions. For example, the same Z-line positions would be used for each probe (an additional variable would be needed to allow for a possible offset due to misregistration of the channels). Similarly, a proportionality parameter or constant may directly relate Z-line weights and Gaussian widths for both probes. This modification would require simultaneously modeling all of the line scans with multiple myofibril intensity profiles. By relying on the known structure of the myofibril, this modification would significantly decrease the number of parameters used to model the Z-lines positions and weights. The reduced number of parameters would improve the data/parameter ratio and help ensure that a particular model was not over-fitting the data.

In conclusion, distributed deconvolution provides a new tool to measure thin filament lengths accurately and precisely in a variety of conditions. It is a flexible and powerful method that can be applied to many probes and distributions.

APPENDIX

The myofibril line scan is the 1D fluorescence intensity distribution of a myofibril. The intensity observed at any point x along the myofibril line scan is $I(x)$. The myofibril profile is a model of the myofibril line scan that is calculated from the values of specific parameters. The intensity at any point x along the myofibril profile is $J(x)$. The residual $R(x)$ is the difference between the observed intensity of the myofibril line scan and the calculated intensity of the myofibril profile. Thus,

$$R(x) = I(x) - J(x). \tag{A1}$$

The goal of distributed deconvolution is to determine the parameters for $J(x)$ that minimizes the residuals along the myofibril. This appendix describes the equations and parameters that constitute the myofibril profile $J(x)$ and the equations used to fit and evaluate the model.

Distributed deconvolution describes the myofibril profile $J(x)$ as a convolution of three independent fluorescent intensity-distribution functions: the Gaussian distribution function $G(x)$, the thin filament distribution function $S(x)$, and Z-line distribution function $Z(x)$. Thus,

$$J(x) = G(x) \otimes S(x) \otimes Z(x) \tag{A2}$$

where $\otimes$ is convolution. These functions are continuous along the x axis. However, because the myofibril line scan is digital, each function is also digitized. Each distribution function and its digitization method is described below.

The Gaussian distribution function $G(x)$ is defined by a normal distribution function centered at the origin. For any position x, the intensity $G(x)$ is determined by the value of the Gaussian width parameter, f, which corresponds to the standard deviation of the normal distribution,

$$G(x, f) = \frac{1}{f\sqrt{2\pi}} e^{-x^2/2f^2}. \tag{A3}$$

Because the area under the Gaussian distribution is one for all values of f, the Gaussian distribution function describes how fluorescence intensity from each pixel is redistributed to neighboring pixels. Large values of the Gaussian width parameter f redistribute the intensities more than small values. The Gaussian distribution function is automatically digitized in Excel using the NORMDIST function, with a mean of zero, and a standard deviation of f. The Gaussian distribution was typically evaluated from $x = (-16, 16)$ because this range accounts for greater than 99.9% of the distribution when the Gaussian width is less than 5.0. The range was increased when the Gaussian width exceeded 5.0, such that at least 99.9% of the distribution was included.

The Z-line distribution $Z(x)$ is a "comb" distribution that determines the location and weight (total intensity) of the thin filament components along the myofibril. The comb distribution is a modified Dirac delta distribution that has multiple nonzero values corresponding to Z lines. For each Z line included within 5 pixels of the myofibril region being modeled, there are two parameters (ζ, w) that determine its position and weight. The position of the first Z line (from the left) is determined by ζ_1 and its weight by w_1;

the position of the second Z line is determined by ζ_2 and its weight by w_2, and so on. Thus, for a Z-line distribution containing n Z lines,

$$Z(x, \zeta_1, w_1, \zeta_2, w_2, \ldots, \zeta_n, w_n) = \begin{cases} w_1, & \text{for } x = \zeta_1 \\ w_2, & \text{for } x = \zeta_2 \\ \vdots & \\ w_n, & \text{for } x = \zeta_n \\ 0, & \text{for all other } x. \end{cases} \quad \text{(A4)}$$

The Z-line distribution function is digitized according to the following method. If a Z line of weight w is located at ζ, between pixels i and $i + 1$, it is digitized such that

$$Z(i) = w(i + 1 - \zeta)$$

and

$$Z(i + 1) = w(\zeta - i). \quad \text{(A5)}$$

For example, a Z line of weight 100 at pixel 10.7 would be digitized such that $Z(10) = 30$ and $Z(11) = 70$. A Z line of weight 200 at pixel 20.2 would be digitized such that $Z(20) = 160$ and $Z(21) = 40$. This digitization method requires that two or more pixels separate all Z lines.

The thin filament distribution function $S(x)$ determines the distribution of fluorescence within an individual thin filament array. The function is symmetric about the Z line ($x = 0$). For any position x, the intensity $S(x)$ is determined by three parameters: u, p, L, such that

$$S(x, p, u, L) = \begin{cases} 1, & \text{for } x = 0 \quad \text{(Z line)} \\ u, & \text{for } -L < x < 0 \text{ or } 0 < x < L \\ p + u, & \text{for } x = -L \text{ or } x = L \quad \text{(P ends)} \\ 0, & \text{for } x < -L \text{ or } x > L\,. \end{cases} \quad \text{(A6)}$$

The parameter u is uniform intensity along the length of the thin filament relative to the Z line, and the parameter p is the intensity at the pointed ends of the thin filament relative to the Z line. The parameters u and p are constrained to be non-negative. The parameter L determines how far the uniform intensity extends from the Z line and the location of the pointed ends with respect to the Z line, and thus corresponds to the lengths of the thin filaments. This parameter was normally allowed to vary between 3 and 15 pixels. However, this range can be changed depending on the magnification and the lengths of the thin filaments.

Although this thin filament distribution function is used for each thin filament component, only two parameters are allowed to vary at a time while the third remains constant. For the Tmod thin filament distribution, u is held constant at one while the parameters p and L may vary. In this case, the P/U ratio is equal to p. For the phallacidin and α-actinin thin filament distributions, p is held constant at zero while the parameters u and L may vary. In these cases, the Z/U ratio for phallacidin is equal to $1/u$ and the U/Z ratio for α-actinin is equal to u.

Because L can be nonintegral, the thin filament distribution function is digitized at the pointed ends based on the same principle used to digitize the Z line distribution function. Thus, when L is between pixels i and $i + 1$,

$$S(i, p, u, L) = \begin{cases} \mu(L - (i - 0.5)) + p(i + 1 - L) \\ \qquad \text{for } i < L < i + 0.5 \\ u + p(i + 1 - L) \\ \qquad \text{for } i + 0.5 < L < i + 1. \end{cases} \quad \text{(A7a)}$$

and

$$S(i + 1, p, u, L) = \begin{cases} p(L - i) \\ \qquad \text{for } i < L < i + 0.5 \\ u(L - (i + 0.5)) + p(L - i) \\ \qquad \text{for } i + 0.5 < L < i + 1. \end{cases} \quad \text{(A7b)}$$

The three distribution functions are convoluted after they are digitized. First, the Gaussian distribution $G(x)$ is convoluted with the thin filament distribution $S(x)$ to generate the thin filament intensity profile $F(x)$,

$$F(x) = G(x, f) \otimes S(x, p, u, L), \text{ for } x = \ldots, -1, 0, 1, \ldots$$
$$= \sum_{n=-\infty}^{\infty} G(n, f) \times S(n + x, p, u, L). \quad \text{(A8a)}$$

Because the Gaussian distribution is typically evaluated over $x = (-16, 16)$ and $S(x) = 0$ when $x > 15$ or $x < 15$ because of the constraints on L, then,

$$F(x) = \sum_{n=-16}^{16} G(n, f) \times S(n + x, p, u, L). \quad \text{(A8b)}$$

If the constraints on L change because of the magnification or lengths of the thin filaments or if the Gaussian width is more than 5.0, then Eq. A8b must be modified to include more terms. In all cases, enough terms were used to account for at least 99.9% of the thin filament profile.

Second, the thin filament profile $F(x)$ is convoluted with the Z-line distribution $Z(x)$ to generate the myofibril profile $J(x)$,

$$J(x) = F(x, f, u, p, L) \otimes Z(x, \zeta_1, w_1, \ldots, \zeta_n, w_n)$$
$$= \sum_{m=-\infty}^{\infty} F(m, f, u, p, L) \cdot Z(m + x, \zeta_1, w_1, \ldots, \zeta_n, w_n). \quad \text{(A9a)}$$

Because 99.9% of $F(x)$ is typically contained within the region $x = (-25, 25)$, Eq. A9a is simplified to

$$J(x) = \sum_{m=-25}^{25} F(m, f, u, p, l) \cdot Z(m + x, \zeta_1, w_1, \ldots, \zeta_n, w_n). \quad \text{(A9b)}$$

However, more terms are included to ensure that at least 99.9% of $F(x)$ is accounted.

The parameters for the Gaussian, thin filament, and Z-line distributions were determined using the Excel Solver Add-in to minimize a normalized error function E. For a myofibril line scan with n pixels and a maximum intensity I_{max}, the error of the myofibril profile is

$$E = \frac{1}{I_{max}} \frac{1}{n} \sqrt{\sum_{x=0}^{n} R(x)^2}\,. \quad \text{(A10)}$$

The error function is similar to a correlation coefficient except that the residuals are minimized independently of line scan intensity, consistent with a uniform level of noise associated with a CCD image.

The R-factor R determines how poorly a myofibril profile fits to a myofibril line scan

$$R = \sum_{x=0}^{n} |R(x)| \Big/ \sum_{x=0}^{n} I(x). \tag{A11}$$

It should also be noted that the total area under the myofibril line scan is

$$\text{Area} = \sum_{x=0}^{n} I(x), \tag{A12}$$

whereas the area under the myofibril profile is

$$\text{Area} = \sum_{x=0}^{n} J(x). \tag{A13}$$

Finally, the width of the Z line can be determined from the Z/U ratio parameter by the equation,

$$\text{Z line width} = (\text{Z/U ratio} - 1) \times (\text{pixel size}). \tag{A14}$$

We thank Elizabeth Getzoff, Brian Dominy, and Chris Putman for help with developing the model and methods for statistical analysis. We thank David DeRosier for suggesting the use of R-factors.

R.S.L. was a recipient of a Pre-doctoral Fellowship from the American Heart Association, Western States Affiliate. This work was supported by grants to V.M.F. from the National Institutes of Health (GM 34225) and from the Human Frontiers in Science Program.

REFERENCES

Agard, D. A., Y. Hiraoka, P. Shaw, and J. W. Sedat. 1989. Fluorescence microscopy in three dimensions. *Methods Cell Biol.* 30:353–377.

Almenar-Queralt, A., C. C. Gregorio, and V. M. Fowler. 1999a. Tropomodulin assembles early in myofibrillogenesis in chick skeletal muscle: evidence that thin filaments rearrange to form striated myofibrils. *J. Cell Sci.* 112:1111–1123.

Almenar-Queralt, A., A. Lee, C. A. Conley, L. Ribas de Pouplana, and V. M. Fowler. 1999b. Identification of a novel tropomodulin isoform, skeletal tropomodulin, that caps actin filament pointed ends in fast skeletal muscle. *J. Biol. Chem.* 274:28466–28475.

Ao, X., and S. S. Lehrer. 1995. Phalloidin unzips nebulin from thin filaments in skeletal myofibrils. *J. Cell Sci.* 108:3397–3403.

Bukatina, A. E., F. Fuchs, and S. C. Watkins. 1996. A study on the mechanism of phalloidin-induced tension changes in skinned rabbit psoas muscle fibres. *J. Muscle Res. Cell Motil.* 17:365–371.

Burkholder, T. J., and R. L. Lieber. 2001. Sarcomere length operating range of vertebrate muscles during movement. *J. Exp. Biol.* 204: 1529–1536.

Cano, M. L., L. Cassimeris, M. Joyce, and S. H. Zigmond. 1992. Characterization of tetramethylrhodaminyl-phalloidin binding to cellular F-actin. *Cell Motil. Cytoskel.* 21:147–158.

Dabiri, G. A., K. K. Turnacioglu, J. M. Sanger, and J. W. Sanger. 1997. Myofibrillogenesis visualized in living embryonic cardiomyocytes. *Proc. Natl. Acad. Sci. U.S.A.* 94:9493–9498.

De La Cruz, E., and T. D. Pollard. 1994. Transient kinetic analysis of rhodamine phalloidin binding to actin filaments. *Biochemistry.* 33: 14387–14392.

Fowler, V. M., M. A. Sussmann, P. G. Miller, B. E. Flucher, and M. P. Daniels. 1993. Tropomodulin is associated with the free (pointed) ends of the thin filaments in rat skeletal muscle. *J. Cell Biol.* 120:411–420.

Gelles, J., B. J. Schnapp, and M. P. Sheetz. 1988. Tracking kinesin-driven movements with nanometre-scale precision. *Nature.* 331:450–453.

Granzier, H. L., H. A. Akster, and H. E. Ter Keurs. 1991. Effect of thin filament length on the force–sarcomere length relation of skeletal muscle. *Am. J. Physiol. Cell Physiol.* 260:C1060–C1070.

Gregorio, C. C., and V. M. Fowler. 1995. Mechanisms of thin filament assembly in embryonic chick cardiac myocytes: tropomodulin requires tropomyosin for assembly. *J. Cell Biol.* 129:683–695.

Holtzer, H., T. Hijikata, Z. X. Lin, Z. Q. Zhang, S. Holtzer, F. Protasi, C. Franzini-Armstrong, and H. L. Sweeney. 1997. Independent assembly of 1.6 microns long bipolar MHC filaments and I-Z-I bodies. *Cell Struct. Funct.* 22:83–93.

Huxley, H. E. 1963. Electron microscope studies on the structure of natural and synthetic protein filaments from striated muscle. *J. Mol. Biol.* 7:281–308.

Knight, P. J., and J. A. Trinick. 1982. Preparation of myofibrils. *Methods Enzymol.* 85:9–12.

Kouchi, K., H. Takahashi, and Y. Shimada. 1993. Incorporation of microinjected biotin-labelled actin into nascent myofibrils of cardiac myocytes: an immunoelectron microscopic study. *J. Muscle Res. Cell Motil.* 14:292–301.

Kruger, M., J. Wright, and K. Wang. 1991. Nebulin as a length regulator of thin filaments of vertebrate skeletal muscles: correlation of thin filament length, nebulin size, and epitope profile. *J. Cell Biol.* 115: 97–107.

Littlefield, R., A. Almenar-Queralt, and V. M. Fowler. 2001. Actin dynamics at pointed ends regulates thin filament length in striated muscle. *Nature Cell Biol.* 3:544–551.

Littlefield, R., and V. M. Fowler. 1998. Defining actin filament length in striated muscle: rulers and caps or dynamic stability? *Annu. Rev. Cell Dev. Biol.* 14:487–525.

Lu, M. H., C. DiLullo, T. Schultheiss, S. Holtzer, J. M. Murray, J. Choi, D. A. Fischman, and H. Holtzer. 1992. The vinculin/sarcomeric-alpha-actinin/alpha-actin nexus in cultured cardiac myocytes. *J. Cell Biol.* 117:1007–1022.

Ohtsuki, I. 1979. Number of anti-troponin striations along the thin filament of chick embryonic breast muscle. *J. Biochem. (Tokyo).* 85:1377–1378.

Ojima, K., Z. X. Lin, Z. Q. Zhang, T. Hijikata, S. Holtzer, S. Labeit, H. L. Sweeney, and H. Holtzer. 1999. Initiation and maturation of I-Z-I bodies in the growth tips of transfected myotubes. *J. Cell Sci.* 112:4101–4112.

Page, S. G., and H. E. Huxley. 1963. Filament lengths in striated muscle. *J. Cell Biol.* 19:369–390.

Robinson, T. F., and S. Winegrad. 1979. The measurement and dynamic implications of thin filament lengths in heart muscle. *J. Physiol. (Lond).* 286:607–619.

Sanger, J. M., B. Mittal, M. B. Pochapin, and J. W. Sanger. 1986. Myofibrillogenesis in living cells microinjected with fluorescently labeled alpha-actinin. *J. Cell Biol.* 102:2053–2066.

Sosa, H., D. Popp, G. Ouyang, and H. E. Huxley. 1994. Ultrastructure of skeletal muscle fibers studied by a plunge quick freezing method: myofilament lengths. *Biophys. J.* 67:283–292.

Squire, J. M. 1997. Architecture and function in the muscle sarcomere. *Curr. Opin. Struct. Biol.* 7:247–257.

Trombitas, K., L. Frey, and G. H. Pollack. 1993. Filament lengths in frog semitendinosus and tibialis anterior muscle fibres. *J. Muscle Res. Cell Motil.* 14:167–172.

van Leeuwen, J. L. 1991. Optimum power output and structural design of sarcomeres. *J. Theor. Biol.* 149:229–256.

Vigoreaux, J. O. 1994. The muscle Z band: lessons in stress management. *J. Muscle Res. Cell Motil.* 15:237–255.

Zhukarev, V., J. M. Sanger, J. W. Sanger, Y. E. Goldman, and H. Shuman. 1997. Distribution and orientation of rhodamine-phalloidin bound to thin filaments in skeletal and cardiac myofibrils. *Cell Motil. Cytoskel.* 37: 363–377.